

SCIENTIFIC REPORTS



OPEN

Broadband perfect light trapping in the thinnest monolayer graphene-MoS₂ photovoltaic cell: the new application of spectrum-splitting structure

Yun-Ben Wu^{1,2}, Wen Yang³, Tong-Biao Wang², Xin-Hua Deng² & Jiang-Tao Liu^{1,2}

The light absorption of a monolayer graphene-molybdenum disulfide photovoltaic (GM-PV) cell in a wedge-shaped microcavity with a spectrum-splitting structure is investigated theoretically. The GM-PV cell, which is three times thinner than the traditional photovoltaic cell, exhibits up to 98% light absorptance in a wide wavelength range. This rate exceeds the fundamental limit of nanophotonic light trapping in solar cells. The effects of defect layer thickness, GM-PV cell position in the microcavity, incident angle, and lens aberration on the light absorptance of the GM-PV cell are explored. Despite these effects, the GM-PV cell can still achieve at least 90% light absorptance with the current technology. Our proposal provides different methods to design light-trapping structures and apply spectrum-splitting systems.

Nano-sized photovoltaic cells have attracted significant attention because of their low cost and high efficiency^{1–14}. Working medium materials such as monocrystalline Si account for over 40% of the total cost of a traditional photovoltaic cell. Therefore, reducing the thickness of the working medium decreases the cost of photovoltaic cells. In optoelectronic devices such as photovoltaic cells and photoelectric detectors, the thickness of the working medium layer should be lower than the diffusion length of the carriers to reduce the losses induced by photon-generated carrier recombination^{1,2}. Nano-sized photovoltaic cells can be synthesized using low-mobility materials, such as amorphous silicon and organic semiconductor materials, to reduce further the cost^{1,2}. Decreasing the thickness of photovoltaic cells reduces the losses induced by photon-generated carrier recombination and thus enhances photoelectric conversion efficiency. Bernardi *et al.* proposed an ultrathin photovoltaic cell (i.e., about 1 nm thick) composed of monolayer graphene and monolayer MoS₂¹⁰. The light conversion efficiency per unit of mass of this photovoltaic cell is three orders of magnitude higher than that of the traditional photovoltaic cell. Since the discovery of this ultrathin photovoltaic cell, different types of photovoltaic cells based on 2D materials have been proposed^{15–19}. However, the light absorptance of the monolayer graphene-molybdenum photovoltaic (GM-PV) cell is only about 10%. Thus, a light-trapping structure should be employed to optimize the light absorption of the GM-PV cell.

A light-trapping structure with an effective design is critical to increase light absorption in nano-sized photovoltaic cells. In general, a light-trapping structure is not designed on the basis of light interference and exhibits a poor light-trapping efficiency. Broadband perfect absorption can hardly be achieved in a < 300 nm thick medium layer because of the limitations of Lambertian light trapping^{1–4}. Moreover, an anti-reflection layer with the thickness of several micrometers should be added^{1–4}. A strong light localization can be realized with an interference-based light-trapping structure (i-LTS), which can greatly enhance the light absorption and simultaneously reduce the reflection of a semiconductor^{3,4,20–30}. Therefore, an additional anti-reflection layer is no longer needed. In consideration of the fundamental limit of nanophotonic light trapping in solar cells^{2,3}, a strong absorption can hardly be achieved at the full spectrum of sunlight. However, the resonant frequency of i-LTS

¹Nanoscale Science and Technology Laboratory, Institute for Advanced Study, Nanchang University, Nanchang 330031, China. ²Department of Physics, Nanchang University, Nanchang 330031, China. ³Beijing Computational Science Research Center, Beijing 100094, China. Correspondence and requests for materials should be addressed to J.-T.L. (email: jtliu@semi.ac.cn)

can usually be adjusted by changing a characteristic parameter, such as the cavity length and the lattice constant of the photonic crystal. Therefore, employing a spectrum-splitting structure can focus sunlight with different wavelengths onto a light-trapping structure with different characteristic parameters to enhance light absorption through resonance in a wide frequency range.

A spectrum-splitting structure is widely applied in super-efficient photovoltaic cells^{31–35}. This structure can reduce the thermal losses caused by the mismatch between the photon energy and the semiconductor's band gap by focusing light with different wavelengths on semiconductors with various band gaps^{31–35}. Thermal losses may be reduced to approximately 10% by using 8–10 semiconductors with different band gaps to constitute a photovoltaic cell³². In our previous studies, we combined the spectrum-splitting structure and the resonance back-reflection light trapping structure to achieve broadband perfect absorption in a semiconductor film with a thickness of approximately 100 nm³⁶. However, light localization is weak in the resonance back-reflection light trapping structure. Hence, perfect light absorption can hardly be achieved in a 1 nm thick medium layer. Demands on material mobility can be minimized by reducing the thickness of the medium layer to ~1 nm, and the energy band structure and optical properties of a ~1 nm semiconductor film can be controlled by adjusting structural and physical parameters such as stress. This process promotes the applications of energy band engineering in photovoltaic cells.

Several recent studies have explored the enhanced absorption of light in 2D materials such as graphene by using various optical microstructures^{37–49}. In the present study, we combined an asymmetric photonic crystal microcavity with a wedge-shaped defect layer and spectrum-splitting structure. Using this structure produced a GM-PV cell that is three times thinner than the traditional photovoltaic cell and that exhibits a preferable light absorptance higher than 98% in a wide wavelength range. We also determined the effects of defect layer thickness, GM-PV cell position in the microcavity, incident angle, and lens aberration on the light absorption rate of the GM-PV cell to compare the calculation results and the actual outcome. Despite these effects, the light absorptance of the GM-PV cell can exceed 90% with the current technology. The study provides different methods to design light-trapping structures and apply spectrum-splitting systems.

Results

The effect of the common microcavity on the absorptance of the GM-PV cell is presented to understand the physical mechanism and show the advantages and disadvantages of traditional i-LTS. Figure 1(a) shows the structure of a common microcavity. The cyan layer, blue layer, and the red layer is the SiO₂ layer, ZnS layer, and the GM-PV cell layer, respectively. The defect layer with dielectric n_c is in the middle of the cavity, and the GM-PV cell is at the center of the defect layer. The distributed Bragg reflectors (DBRs) in which two materials with different dielectric (n_1 and n_2) are alternately distributed are on both sides of the cavity with periodicities of M_1 and M_2 . $n_c = n_1 = 1.55$ (e.g., SiO₂) and $n_2 = 2.59$ (e.g., ZnS) are used in the calculation. The corresponding layer thicknesses are $d_1 = \lambda_{DBR}/4n_1$ and $d_2 = \lambda_{DBR}/4n_2$, where λ_{DBR} is the center wavelength. All layers are nonmagnetic ($\mu = 1$). For a direct comparison, the light absorptivities of the monolayer graphene, MoS₂, and GM-PV cell were calculated. The refractive index of graphene can be expressed as $n_g = 3.0 + C_{1/3} \frac{\lambda}{i}$, where $C_{1/3} = 5.446 \mu\text{m}^{-1}$, and the thickness of the graphene monolayer can be expressed as $d_g = 0.34 \text{ nm}^{50}$. The data of MoS₂ are obtained from ref. 51. The results are presented in Fig. 1(b). The absorptance of the GM-PV cell is approximately 10%, increases rapidly at short wavelengths, and reaches 30%. Previous studies reported that using an asymmetric microcavity can reduce reflection and enhance light absorption³⁹. We calculated the absorptance at wavelengths of 470 and 610 nm [Fig. 1(c,d)] as the periodicity of the DBRs on both sides of the microcavity varies. At 470 nm, the GM-PV cell exhibits a high absorptance, and the required Q-value is small. When $M_1 = 2$ and $M_2 > 5$, the absorption is almost saturated. At 610 nm, the GM-PV cell exhibits a low absorptance, and the required Q-value is large. When $M_1 = 3$ and $M_2 > 6$, the absorption is basically saturated. The changes in absorptance with varying wavelengths are presented in Fig. 1(e). The maximum absorptance is 98.5%, and the full width at half maximum (FWHM) is 20.2 nm. In this structure, the absorptance is close to 1 is because interference can reduce the reflection, and light can be reflected in the microcavity for multiple times, causing a strong light localization [inset of Fig. 1(e)].

The resonance state in the microcavity is sensitive to the thickness of the defect layer and the incident angle. The calculated results are illustrated in Fig. 1(f–h). The resonant wavelength of the microcavity satisfies $m_i \lambda_c / 2 = L_c \cos \theta'$, where $L_c = n_c d_c$ denotes the optical path of the microcavity, n_c and d_c are the refractive index and the thickness of the defect layer, respectively; m_i is the positive integer; and $\theta' = \arcsin \theta_i / n_c$ signifies the propagation angle of the light in the defect layer, where θ_i is the incident angle. Thus, the resonant wavelength linearly increases as the defect layer thickness increases. Then, the resonant wavelength moves toward the direction of the short wave as the incident angle increases. Perfect absorption is mainly distributed at the photonic band gap (470–670 nm) because the thickness of the photonic crystals on both sides remains unchanged. The resonant wavelength also correlates with the propagation angle in the defect layer. The higher the refractive index of the defect layer, the smaller the propagation angle. Accordingly, minimal changes in the resonance peak occur as the incident angle varies. In the calculations, the resonance peak is sensitive to the incident angle when the refractive index of the defect layer is 1.55. The resonance absorption peak slightly shifts when the incident angle is 15°. Comparatively, the resonance peak shifts with a distance up to a FWHM when the incident angle is 30°.

Basing from the calculation results, we can conclude that the light absorption of the GM-PV cell in a common photonic crystal microcavity can only be enhanced at some specific wavelengths. In other words, the method cannot be directly applied in photovoltaic cells. However, the microcavity-based resonant wavelength linearly increases as the defect layer thickness increases. Therefore, a wedge-shaped defect layer is introduced, and sunlight with different wavelengths can be focused onto different positions in the microcavity through the spectrum-splitting structure. The resonance absorption of light can be achieved at the position where light is focused because of the appropriate thickness distribution of the defect layer [Fig. 2(a)]. Accordingly, resonance-induced absorption enhancement can be realized in a broad frequency range. The spectrum-splitting

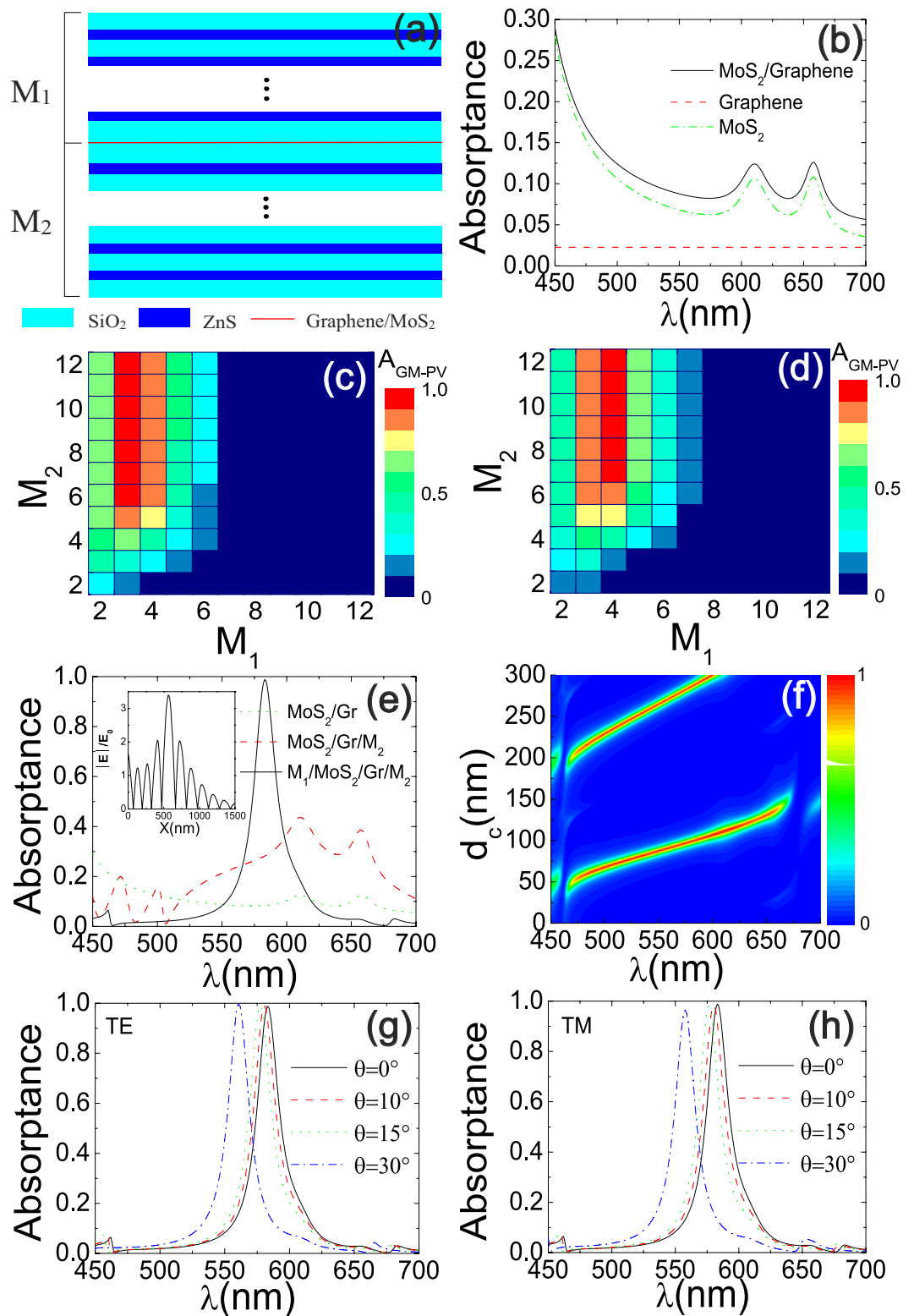


Figure 1. (a) Schematic of a common photonic crystal microcavity. The cyan layer, blue layer, and the red layer is the SiO₂ layer, ZnS layer, and the GM-PV cell layer, respectively. (b) Light absorbance of the monolayer graphene, MoS₂, and GM-PV cell. (c) Absorbance of the GM-PV cell (A_{GM-PV}) as a function of the periodicity of the distributed Bragg reflectors on both sides of the microcavity at wavelengths of (c) 470 nm and (d) 610 nm. (e) Absorbance variation of the GM-PV cell in the microcavity at different wavelengths (inset: light field distribution). (f) Contour chart of the absorbance of the GM-PV cell at different wavelengths and of the thickness of the defect layer. Absorbance variation of the GM-PV cell with changing wavelengths at different incident angles: (g) TE mode and (h) TM mode.

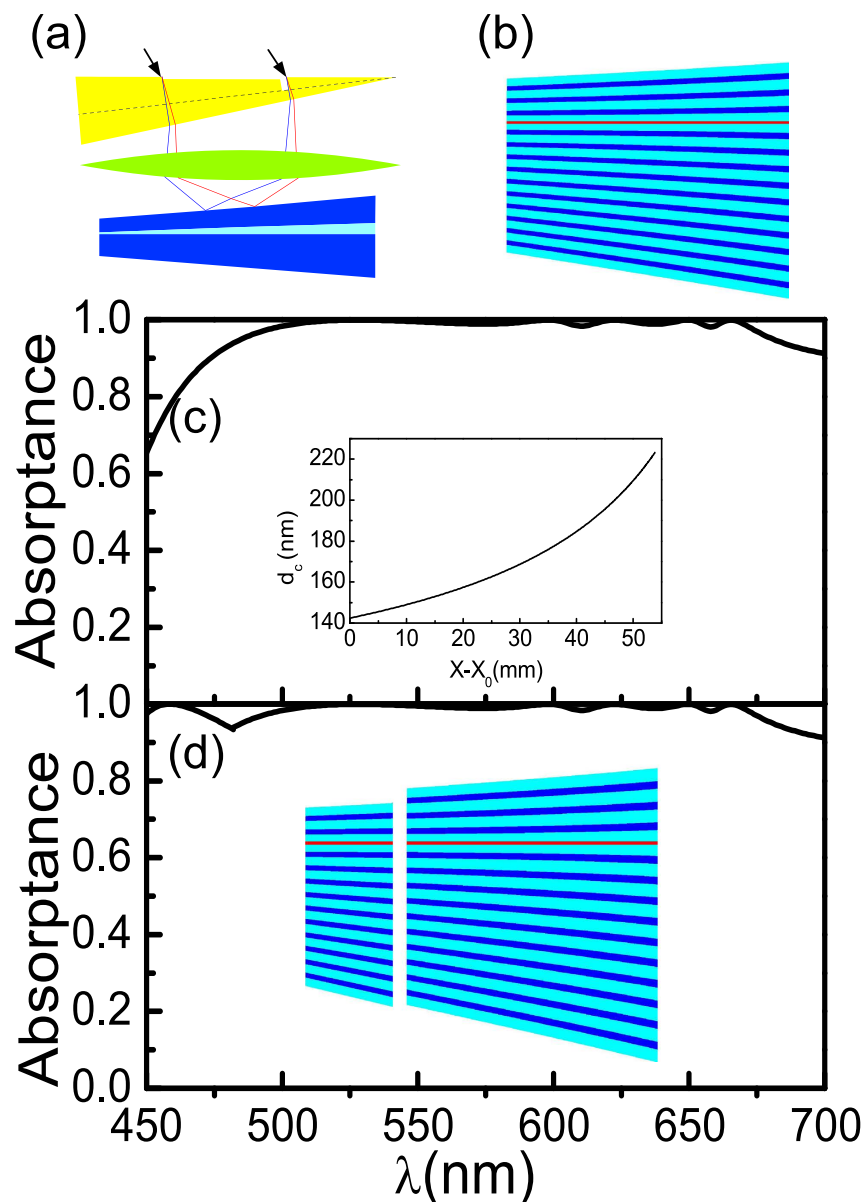


Figure 2. Schematic of the (a) spectrum-splitting system and (b) wedge-shaped photonic crystal; (c) absorbance of the GM-PV cell in the wedge-shaped microcavity (inset: thickness variation of the defect layer with varying position coordinates); (d) absorbance of the GM-PV cell in the split wedge-shaped microcavity (inset: shoulder-to-shoulder wedge-shaped microcavity).

structure is composed of a dense flint ZF13 prism and a low dispersion convex lens. The refractive index for ZF13 glass is $n_{ZF13}^2 = z_{g1} - z_{g2}\lambda^2 + z_{g3}\lambda^{-2} + z_{g4}\lambda^{-4} - z_{g5}\lambda^{-6} + z_{g6}\lambda^{-8}$, where $z_{g1} = 3.05344$, $z_{g2} = 1.2752 \times 10^{-2}$, $z_{g3} = 4.0609 \times 10^{-2}$, $z_{g4} = 2.2706 \times 10^{-3}$, $z_{g5} = 7.8087 \times 10^{-5}$, and $z_{g6} = 1.9874 \times 10^{-5}$. Similarly, the DBRs on both sides of the microcavity are wedge-shaped to further increase the band gap [Fig. 2(b)].

Figure 2(c) presents the calculation results, in which the periodicities of the upper and lower DBRs are 3 and 10, respectively. The slope of the wedge-shaped layer is about 1.4×10^{-6} ; hence, the layers can be treated as parallel planes at each point. Thus, the transfer matrix method can be used in the calculation (Supplementary Information S1). Light with different wavelength incidents on different positions in the microcavity through the spectrum-splitting structure can achieve a resonance-induced absorption enhancement by adjusting the thickness of the defect layer. The calculated thickness distribution of the resonance defect layer is presented in the inset of Fig. 2(c). In this system, the absorbance of the GM-PV cell can exceed 98% at a wavelength of 500–670 nm (i.e., 670 nm at approximately the band gap of the monolayer MoS₂) by combining the spectrum-splitting structure and i-LTS. The absorbance of the GM-PV cell significantly decreases when the wavelength is less than 500 nm. This result can be attributed to the strong absorption of the GM-PV cell at short wavelengths and the large periodicity of the DBR. These features can suppress interference, increase reflection, and reduce absorbance [Fig. 1(c)]. Nevertheless, shoulder-to-shoulder microcavities with different Q-values can be used in the design [inset of Fig. 2(d)] similar to the design of the shoulder-to-shoulder sub-batteries adopted in common spectrum-splitting

systems. Light absorption at wavelengths less than 500 nm can be enhanced by reducing the periodicity of the upper DBR [Fig. 2(d)]. The DBR can also be fabricated with parallel layers by using the shoulder-to-shoulder microcavities (Supplementary Information S2). Some position might absorb less energy depending on the solar spectrum. However, different from the traditional photovoltaic cell with a spectrum-splitting structure, the GM-PV cell is ultra-thin. The photo-generated electrons and holes can be collected rapidly by the electrode. The space charge accumulation is weak in the GM-PV cell.

To associate the calculation results with practical production, the effects of GM-PV cell location in the microcavity, defect layer thickness, incident angle, and lens aberration on the absorptance of the GM-PV cell are further investigated. The calculation results are presented in Fig. 3. Other effects such as the influence of the fabrication tolerances of the photonic crystal (Supplementary Information S3), outermost layer correction (Supplementary Information S4), and the tolerances of the photovoltaic cells position (Supplementary Information S5) are shown in the supplementary materials.

Light localization is the strongest at the center of the cavity. The absorptance of the GM-PV cell declines when it is off-center. Nevertheless, the absorptance at the off-center position is slightly affected because the light field is almost evenly distributed in the cavity. The absorptance of the GM-PV cell exhibits almost no variation at $\Delta Z = 10$ nm, slightly varies at $\Delta Z = 20$ nm, and significantly declines at $\Delta Z \geq 30$ nm. The absorptance change increases at short wavelengths. This result can be attributed to the fact that a thinner defect layer at short wavelengths leads to a greater relative deviation. A change in defect layer thickness influences the absorptance of the GM-PV cell. The resonant frequency of the microcavity varies as the defect layer thickness varies. Thus, the resonance-induced perfect absorption of the light incident on the cavity can no longer be achieved, i.e., the absorptance is reduced. The absorptance slightly changes when the variation amplitude of the defect layer thickness is 1 nm. The light absorptance at > 500 nm wavelengths significantly decreases when the variation amplitude of the thickness is 2 nm. However, it can still exceed 90%. The light absorptance at < 500 nm wavelengths shows almost no change because of the lower Q-value of the microcavity. The light localization becomes weaker and the FWHM increases as the Q-value decreases. The tolerance of film growth can be less than 1 nm or even as low as the thickness of an atomic layer because of the development of material growth techniques such as molecular beam epitaxy (MBE).

As described earlier, varying incident angles can change the resonant frequency of the microcavity. Nevertheless, the resonant frequency of the microcavity slightly varies when the incident angle slightly changes. The calculated results are presented in Fig. 3(c,d). The absorptance slightly changes when the variation amplitude of the incident angle is 5° but significantly declines when the incident angle is altered by 10° . The incident angle can be controlled at approximately 0.1° by using the ray tracing system⁵².

Aberration causes the appearance of a light spot after lens imaging. The wavelength perfectly matches with the thickness of the defect layer around the center of the light spot, whereas the wavelength in other positions cannot be matched properly, leading to a decline in absorptance. Figure 3(e,f) present the effects of aberration on the absorptance of the GM-PV cell. Larger lens diameter means larger light spot. Accordingly, mismatch becomes evident, and GM-PV cell absorptance is reduced. The effect of aberration on the absorptance of the GM-PV cell mainly depends on the Q-value and the light-splitting ability of the spectrum-splitting structure. Smaller Q-value means weaker light localization and larger FWHM. Accordingly, the effect of aberration is weak under this condition. In lenses with varying diameters, the absorptance variation at wavelengths less than 500 nm significantly differs from that at wavelengths higher than 500 nm. Figure 3(e,f) show that larger vertical angle of the prism means stronger light-splitting ability and smaller variation gradient. That is, the effect of aberration is minimal.

Discussion

Spectrum-splitting system. The spectrum-splitting structure can reduce the thermal losses caused by the mismatch between the photon energy and the semiconductor's band gap. It can also enhance the light-trapping efficiency via combined utilization with i-LTS. The introduction of the spectrum-splitting structure increases the flexibility of the design of the light-trapping structure. The design of the shoulder-to-shoulder battery can also be adopted. Various light-trapping structures can be selected for sub-batteries with different wavelengths and materials with different band gaps. In addition to the microcavity in the current study, other light-trapping structures can also be employed and combined with the spectrum-splitting structure. These structures include photonic crystal, plasma, and nano-semiconductor-column array with resonant frequencies that are continuously adjustable by some structural parameters. The spectrum-splitting structure studied in this article is composed of disperse prism and convex lens. The structure is simple and can be manufactured easily, which is beneficial to revealing the fundamental principles. However, the light-splitting efficiency is not high, and the system can reflect 15–20% of sunlight. In this case, a highly efficient spectrum-splitting structure should be adopted^{32–35}. The disperse plane lens may be a potential choice⁵³.

Light-trapping ability and technique precision. Theoretically, the light-trapping ability is no limitation in i-LTS combined with the spectrum-splitting structure. However, the practical light-trapping ability is limited to the technique precision. The light-trapping ability of an interference structure can be measured by the Q-value. Larger Q-value means stronger light-trapping ability. Although the Q-value of optical microstructures without absorption can reach up to 10^8 , the light-trapping ability is limited by the processing technique. Basing from the definition of Q-value $Q = \omega_0/\Gamma$, we can conclude that greater Q-values mean smaller FWHM. Meanwhile, smaller FWHM indicates higher demands on the processing precision. For example, with the assumption that the resonant wavelength of the microcavity is $\lambda_c = 2L_c = 2n_c d_c$, resonant wavelength will be changed by $\Delta\lambda_c = 2n_c \Delta d_c$ if d_c is varied to $d_c + \Delta d_c$, because of processing errors, and the absorptance will be reduced by 50% if $\Delta\lambda_c$ reaches half of the FWHM. Thus, after considering processing precision, the light-trapping ability based on the microcavity

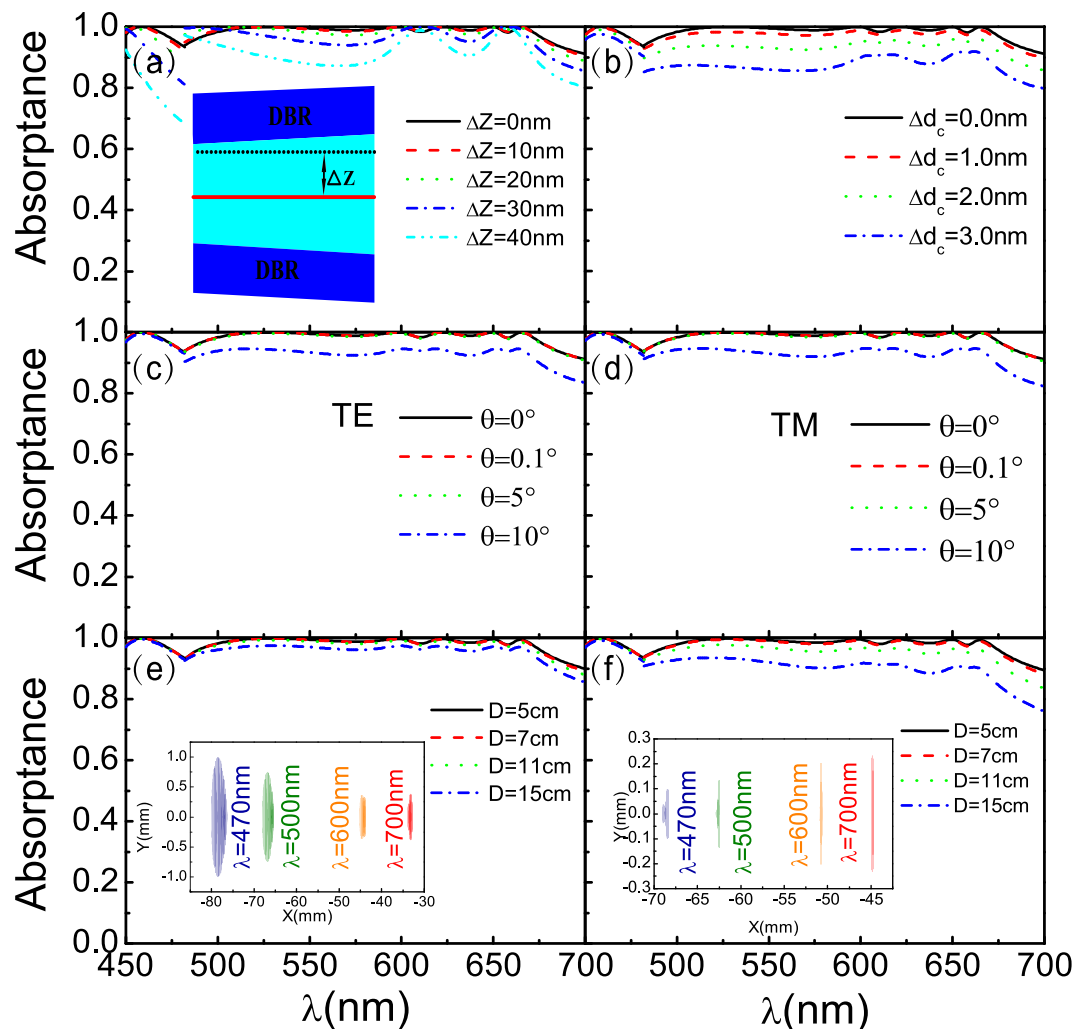


Figure 3. Absorbance of the GM-PV cell at (a) different off-center positions of the GM-PV cell in the microcavity; (b) different defect layer thicknesses; (c) different angles (corresponding to TE mode); (d) different angles (corresponding to TM mode); (e) different lens diameters when the vertex angle of the prism is $\alpha_A = 45^\circ$; (f) different lens diameters when the vertex angle of the prism is $\alpha_A = 30^\circ$; The inset in (e,f) shows a focused light spot of different wavelengths for $D = 15$ and $D = 7$ cm, respectively.

can be increased by at most two to three times than the results of the study. In addition, obtaining the perfect absorption in monolayer graphene with microcavity is difficult to obtain because the light absorption of monolayer graphene is only about 2.3%^{40,41}.

Transparent electrode. On the basis of the strong light localization in i-LTS, the light absorbance of the transparent electrode can be enhanced. Thus, the extinction coefficient of the transparent electrode should be low. The primary problem with the transparent electrode in the traditional photovoltaic cell is that it is required to maintain a small degree of light absorption within the entire spectral region of sunlight. However, different transparent electrodes can be used on sub-batteries by adopting the shoulder-to-shoulder design of the sub-batteries after using the spectrum-splitting structure. These transparent electrodes are only required to exhibit minimal light absorption within a specific frequency range, i.e., the difficulty in the design of the transparent electrode can be significantly reduced.

Materials. This study investigated the light-trapping ability of the thinnest photovoltaic cell (i.e., the graphene-MoS₂ photovoltaic cell) that features the combination of a spectrum-splitting structure and i-LTS. The requirements on material mobility can be minimized because the thickness of the working medium layer is only 1 nm. This phenomenon promotes the application of low-mobility materials, such as noncrystalline materials and organic materials, in photovoltaic cells. When the quantum tunneling effect is considered, an insulating medium with a low barrier height can be used to prepare an absorption medium. In particular, when the thickness of the working medium is reduced to a few nanometers, the energy band structure and optical properties can be adjusted by changing physical and structural parameters, such as stress. Furthermore, the estimated

external quantum efficiency can be increased to larger than 80% by using shoulder-to-shoulder cells consisting of different band gap materials (Supplementary Information S6). This step can largely promote the application of energy-band engineering in photovoltaic cells.

Feasibility of the experiments. The structures can achieve a high light absorptance after considering the present technique precision. The combined utilization of microcavity and traditional semiconductor microstructures, such as quantum well, is mature. The combined utilization of microcavity and 2D materials remains a challenge, but a photonic crystal microcavity that contains graphene has been produced^{40–43}. The primary difficulty in fabricating this product is integrating i-LTS with a spectrum-splitting structure to establish a wedge-shaped medium layer. Prineas *et al.* promoted the growth of 210 wedge-shaped semiconductor layers through MBE to reduce the speed of light⁵⁴. Wedge-shaped microcavities are also widely used in experimental studies of light-matter interactions, such as laser-plasma interactions, cavity polaritons, and Purcell effect^{55–57}.

Limitations. Similar to the traditional spectrum-splitting structure-based photovoltaic cells, the proposed photovoltaic cell is applicable only under direct sunlight. Under indirect sunlight, the conversion efficiency is significantly reduced and the utilization ratio of the scattered sunlight is low. A solar tracker and a feedback mechanical system should be used. In regions with a short period of direct sunlight exposure, the GM-PV cell should be used simultaneously with traditional photovoltaic cells.

In conclusion, broadband perfect absorption can be achieved in the 1 nm-thick GM-PV cell by combining spectrum-splitting structure and i-LTS. The achieved light absorptance exceeds the fundamental limit of nanophotonic light trapping in solar cells. The light absorptance of the GM-PV cell manufactured with the current technology can still exceed 90% regardless of layer thickness errors, the position deviation of the GM-PV cell in the microcavity, deviation of incident angle, and lens aberration. This study not only provides different way to design light-trapping structures and apply spectrum-splitting systems but also have significant applications in the development of optoelectronic devices, such as photoelectric detectors.

Methods

The modified transfer matrix method is used to model the absorption of GM-PV cell in the photonic crystal micro-cavity. For actual convex lens with aberrations, each of the refraction of light through the prism and lens is solved numerically using Snell's law.

References

- Dharmadasa, I. M. (ed.) *Advances in thin-film solar cells* (Pan Stanford Publishing, Boca Raton, 2012).
- Mokkapati, S. & Catchpole, K. R. Nanophotonic light trapping in solar cells. *J. Appl. Phys.* **112**, 101101 (2012).
- Yu, Z., Raman, A. & Fan, S. Fundamental limit of nanophotonic light trapping in solar cells. *PNAS* **107**, 17491–17496 (2010).
- Guo, C. F., Sun, T., Cao, F., Liu, Q. & Ren, Z. Metallic nanostructures for light trapping in energy-harvesting devices. *Light: Science & Applications* **3**, e161 (2014).
- Wallentin, J. *et al.* Inp nanowire array solar cells achieving 13.8% efficiency by exceeding the ray optics limit. *Science* **339**, 1057–1060 (2013).
- Mariani, G., Scofield, A. C., Hung, C.-H. & Huffaker, D. L. Gaas nanopillar-array solar cells employing *in situ* surface passivation. *Nature Communications* **4**, 1497 (2013).
- Krogstrup, P. *et al.* Single-nanowire solar cells beyond the shockley-queisser limit. *Nature Photonics* **7**, 306–310 (2013).
- Nozik, A. J. Nanoscience and nanostructures for photovoltaics and solar fuels. *Nano Lett.* **10**, 2735–2741 (2010).
- Singh, S., Deol, R. S., Singla, M. L. & Jain, D. V. S. Light harvesting efficiency of hybrid nano-composite for photovoltaic application. *Solar Energy Materials and Solar Cells* **128**, 231–239 (2014).
- Bernardi, M., Palummo, M. & Grossman, J. C. Extraordinary sunlight absorption and one nanometer thick photovoltaics using two-dimensional monolayer materials. *Nano Lett.* **13**, 3664–3670 (2013).
- Gong, M. *et al.* Polychiral semiconducting carbon nanotube-fullerene solar cells. *Nano Lett.* **14**, 5308–5314 (2014).
- Battaglia, C. *et al.* Enhanced near-bandgap response in inp nanopillar solar cells. *Advanced Energy Materials* **4**, 1400061 (2014).
- Huang, Z. Y. *et al.* Spontaneous formation of light-trapping nano-structures for top-illumination organic solar cells. *Nanoscale* **6**, 2316–2320 (2014).
- Zhou, L. *et al.* Light manipulation for organic optoelectronics using bio-inspired moth's eye nanostructures. *Scientific Reports* **4**, 4040 (2014).
- Groenendijk, D. J. *et al.* Photovoltaic and photothermoelectric effect in a double-gated wse₂ device. *Nano Lett.* **14**, 5846–5852 (2014).
- Furchi, M. M., Pospischil, A., Libisch, F., Burgdörfer, J. & Mueller, T. Photovoltaic effect in an electrically tunable van der waals heterojunction. *Nano Lett.* **14**, 4785–4791 (2014).
- Tsai, M.-L. *et al.* Monolayer mos₂ heterojunction solar cells. *ACS Nano* **8**, 8317–8322 (2014).
- Shanmugam, M., Jacobs-Gedrim, R., Song, E. S. & Yu, B. Two-dimensional layered semiconductor/graphene heterostructures for solar photovoltaic applications. *Nanoscale* **6**, 12682–12689 (2014).
- Dai, J. & Zeng, X. C. Bilayer phosphorene: Effect of stacking order on bandgap and its potential applications in thin-film solar cells. *J. Phys. Chem. Lett.* **5**, 1289–1293 (2014).
- Wang, K. X. *et al.* Light trapping in photonic crystals. *Energy Environ. Sci.* **7**, 2725 (2014).
- Vynck, K., Burresti, M., Riboli, F. & Wiersma, S. D. Photon management in two-dimensional disordered media. *Nature Materials* **11**, 1017–1022 (2012).
- Martins, E. R. *et al.* Deterministic quasi-random nanostructures for photon control. *Nature Communications* **4**, 2665 (2013).
- Kuo, M. Y. *et al.* Quantum efficiency enhancement in selectively transparent silicon thin film solar cells by distributed bragg reflectors. *Opt. Express* **20**, A828–A835 (2012).
- Loser, S. *et al.* High-efficiency inverted polymer photovoltaics via spectrally tuned absorption enhancement. *Advanced Energy Materials* **4**, 1301938 (2014).
- Rumbak, M., Visoly-Fisher, I. & Shikler, R. Broadband absorption enhancement via light trapping in periodically patterned polymeric solar cells. *J. Appl. Phys.* **114**, 013102 (2013).
- Gan, Q., Bartoli, F. J. & Kafafi, Z. H. Plasmonic-enhanced organic photovoltaics: Breaking the 10% efficiency barrier. *Adv. Mater.* **25**, 2385–2396 (2013).
- Chou, C.-H. & Chen, F.-C. Plasmonic nanostructures for light trapping in organic photovoltaic devices. *Nanoscale* **6**, 8444–8458 (2014), URL <http://dx.doi.org/10.1039/C4NR02191F>.
- Luo, L.-B. *et al.* Light trapping and surface plasmon enhanced high-performance nir photodetector. *Scientific Reports* **4**, 3914 (2014).

29. Lockau, D. *et al.* Advanced microhole arrays for light trapping in thin film silicon solar cells. *Solar Energy Materials and Solar Cells* **125**, 298–304 (2014).
30. Mallick, S. B., Agrawa, M. & Peumans, P. Optimal light trapping in ultra-thin photonic crystal crystalline silicon solar cells. *Optics Express* **18**, 5691–5706 (2010).
31. Goetzberger, A. & Knobloch, J. (eds) *Crystalline Silicon Solar Cells* (John Wiley & Sons, Chichester, 1998).
32. Polman, A. & Atwater, H. A. Photonic design principles for ultrahigh-efficiency photovoltaics. *Nature Materials* **11**, 174–177 (2012).
33. Imenes, A. & Mills, D. Spectral beam splitting technology for increased conversion efficiency in solar concentrating systems: a review. *Solar Energy Materials & Solar Cells* **84**, 19–69 (2004).
34. Barnett, A. *et al.* Very high efficiency solar cell modules. *Prog. Photovolt: Res. Appl.* **17**, 75–83 (2009).
35. Green, M. A. & Ho-Baillie, A. Forty three per cent composite split-spectrum concentrator solar cell efficiency. *Prog. Photovolt: Res. Appl.* **18**, 42–47 (2010).
36. Liu, J.-T., Deng, X.-H., Yang, W. & Li, J. Perfect light trapping in nanoscale thickness semiconductor films with a resonant back reflector and spectrum-splitting structures. *Phys. Chem. Chem. Phys.* **17**, 3303 (2015).
37. Thongrattanasiri, S., Koppens, F. H. L. & de Abajo, F. J. G. Complete optical absorption in periodically patterned graphene. *Phys. Rev. Lett.* **108**, 047401 (2012).
38. Ferreira, A., Peres, N. M. R., Ribeiro, R. M. & Stauber, T. Graphene-based photodetector with two cavities. *Phys. Rev. B* **85**, 115438 (2012).
39. Vincenti, M. A., de Ceglia, D., Grande, M., D'Orazio, A. & Scalora, M. Nonlinear control of absorption in one-dimensional photonic crystal with graphene-based defect. *Opt. Lett.* **38**, 3550–3553 (2013).
40. Furchi, M. *et al.* Microcavity-integrated graphene photodetector. *Nano Lett.* **12**, 2773–2777 (2012).
41. Engel, M. *et al.* Light-matter interaction in a microcavity-controlled graphene transistor. *Nature Communications* **3**, 906 (2012).
42. Schwarz, S. *et al.* Two-dimensional metal chalcogenide films in tunable optical microcavities. *Nano Lett.* **14**, 7003–7008 (2014).
43. Liu, X. *et al.* Strong light-matter coupling in two-dimensional atomic crystals. *Nature Photonics* **9**, 30–34 (2015).
44. Zheng, J., Barton, R. A. & Englund, D. Broadband coherent absorption in chirped-planar-dielectric cavities for 2d-material-based photovoltaics and photodetectors. *ACS Photonics* **1**, 768–774 (2014).
45. Zhang, Z. Z., Chang, K. & Peeters, F. M. Tuning of energy levels and optical properties of graphene quantum dots. *Phys. Rev. B* **77**, 235411 (2008).
46. Zhu, X. *et al.* Experimental observation of plasmons in a graphene monolayer resting on a two-dimensional subwavelength silicon grating. *Appl. Phys. Lett.* **102**, 131101 (2013).
47. Ye, Q. *et al.* Polarization-dependent optical absorption of graphene under total internal reflection. *Appl. Phys. Lett.* **102**, 021912 (2013).
48. Yu, R., Pruneri, V. & de Abajo, F. J. G. Resonant visible light modulation with graphene. *ACS Photonics* **2**, 550–558 (2015).
49. Lien, D.-H. *et al.* Engineering light outcoupling in 2d materials. *Nano Lett.* **15**, 1356–1361 (2015).
50. Bruna, M. & Borini, S. Optical constants of graphene layers in the visible range. *Appl. Phys. Lett.* **94**, 031901 (2009).
51. Liu, J.-T., Wang, T.-B., Li, X.-J. & Liu, N.-H. Enhanced absorption of monolayer MoS_2 with resonant back reflector. *J. Appl. Phys.* **115**, 193511 (2014).
52. Yao, Y., Hu, Y., Gao, S., Yang, G. & Du, J. A multipurpose dual-axis solar tracker with two tracking strategies. *Renewable Energy* **72**, 88–98 (2014).
53. Aieta, F. *et al.* Aberration-free ultrathin flat lenses and axicons at telecom wavelengths based on plasmonic metasurfaces. *Nano Lett.* **12**, 4932–4936 (2012).
54. Prineas, J. P., Johnston, W. J., Yildirim, M., Zhao, J. & Smirl, A. L. Tunable slow light in bragg-spaced quantum wells. *Appl. Phys. Lett.* **89**, 241106 (2006).
55. Schütte, B. *et al.* Continuously tunable laser emission from a wedge-shaped organic microcavity. *Appl. Phys. Lett.* **2008**, 163309 (92).
56. Fleet, L. R., Babiker, M. & Probert, M. I. J. An experiment on the Purcell effect in a wedge cavity. *European Journal of Physics* **30**, S81–S88 (2009).
57. Theobald, W. *et al.* High-intensity laser-plasma interaction with wedge-shaped-cavity targets. *Phys. Plasmas* **17**, 103101 (2010).

Acknowledgements

We would like to thank Nianhua Liu for fruitful discussion. This work was supported by the NSFC (Grant No. 11364033, 11274036, 11322542 and 11264029), the MOST (Grant No. 2014CB848700), and Science and Technology Project of the Education Department of Jiangxi Province (Grant No. GJJ13005).

Author Contributions

Y.-B.W. wrote the program, did the numerical calculation, and analyzed the calculation data. J.-T.L. supervised the project, analyzed the results, and wrote the paper. W.Y. analyzed the results and wrote the paper. T.-B.W. and X.-H.D. helped with analyzed of the results. All authors discussed the results and commented on the manuscript.

Additional Information

Supplementary information accompanies this paper at <http://www.nature.com/srep>

Competing financial interests: The authors declare no competing financial interests.

How to cite this article: Wu, Y.-B. *et al.* Broadband perfect light trapping in the thinnest monolayer graphene- MoS_2 photovoltaic cell: the new application of spectrum-splitting structure. *Sci. Rep.* **6**, 20955; doi: 10.1038/srep20955 (2016).



This work is licensed under a Creative Commons Attribution 4.0 International License. The images or other third party material in this article are included in the article's Creative Commons license, unless indicated otherwise in the credit line; if the material is not included under the Creative Commons license, users will need to obtain permission from the license holder to reproduce the material. To view a copy of this license, visit <http://creativecommons.org/licenses/by/4.0/>